Carbon Nanotube Nucleation Driven by Catalyst Morphology Dynamics

Elena Pigos,[1] Evgeni S. Penev,[2] Morgana A. Ribas,[2] Renu Sharma,[3] Boris I. Yakobson[2,‡] and Avetik R. Harutyunyan[1,*]

[1]*Honda Research Institute USA Inc., Columbus, Ohio 43212*

[2]*Department of Mechanical Engineering & Materials Science and Department of Chemistry, Rice University, Houston, Texas 77005*

[3]*Center for Nanoscale Science and Technology, National Institute of Standards and Technology, Gaithersburg, MD 20899*

In situ observation of the carbon nanotube nucleation process accompanied by dynamic reconstruction of the catalyst particle morphology is considered within a thermodynamic approach, and reveals the driving force for lift-off — a crucial event in nanotube growth. A continuum model and detailed atomistic calculations identify the catalyst surface energy, affected by the chemisorbed carbon atoms at its exterior, and the emergence of a pristine, high-energy facet under the sp^2-carbon dome, as the critical factors in the lift-off process. This further allows evaluation of the range of chemical potential of feedstock, supporting the lift-off process, and provides insights on observed morphology oscillating behavior of the catalyst resulting into formation of multiwall carbon nanotubes.

The materials science of carbon nanotubes (CNT) lies at the intersection of various paradigms from fundamental and applied physics and chemistry. Recognizing how the different concepts can be combined together to understand CNT formation still remains a challenge [1]. There is an overwhelming body of evidence that catalytic growth is the most promising method for CNT synthesis, including the potential for chiral-selectivity [2, 3]. Although knowledge of the different stages of growth has advanced considerably [4], a full picture is still elusive [5]. Mastering chirality control requires a deeper understanding of the very early stage of CNT nucleation, when the symmetry type is set. The system complexity is so great that, in order to explore the details of the growth mechanism at the atomic scale, models are based on either small catalytic particles [6-9] or, at the limit of large catalysts, a slab can be used as an approximation [10, 11]. In more recent experimental studies, especially on growth of multi-walled CNT [12-14], catalyst reshaping has been reported and correlated with surface energy modification due to C adsorption. Studies of the relationship between changes in catalyst particle morphology and CNT nucleation are scarce [15, 16] and a quantitative description is greatly needed.
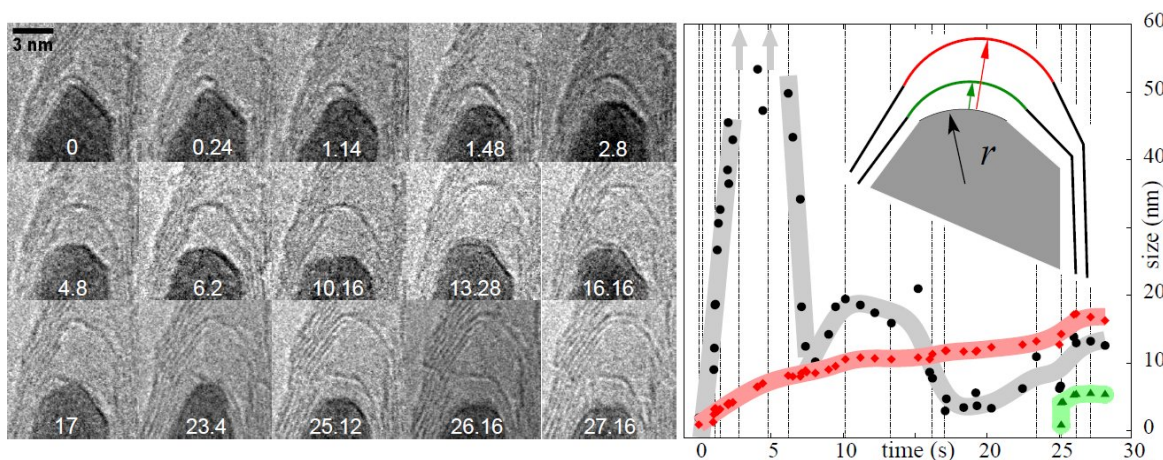

Fig. 1. Evolution of catalyst morphology during CNT nucleation and growth process. Left: Carbon layer attached to the surface of the catalyst particle has just started to split from the top left corner; further lift-off and growth is accompanied by nucleation and expansion of another facet that results in flattening of the top; in the course of the carbon dome lift-off the particle shape under alternates between flatten or rounded; before the particle facet becomes covered by carbon atoms under the dome and the formation of the next carbon dome occurs, the particle shape again becomes more faceted. The process repeats in the course of each new tubular structure formation, following the same lift-off mechanism. The black scale bar on the first image corresponds to $\approx$ 5 nm. Right: The graph shows the dynamics of key dimensions (inset) measured from the sequence of TEM images: the red and the green lines show the distance of the two subsequent sp^2-domes from the top catalyst surface, the grey line shows the radius (r) of curvature of this surface. Vertical lines indicate the times of the snapshots, also marked on each frame (in seconds); estimated error bars are within the size of the symbols.

Targeting this problem, here we report on *in situ* observations of CNT nucleation and growth on metal nanoparticles and put forward a CNT nucleation mechanism based on the lift-off that includes catalyst particle surface energy as a driving force.

2

Results and Discussion

Multi-wall CNTs were grown on a Au-doped Ni catalyst particle at 520 °C by the catalytic chemical vapor deposition (CVD) method from an acetylene (C_2H_2) source in the chamber of a Tecnai F20# environmental scanning/transmission electron microscope (ESTEM) equipped with an electron energy-loss spectrometer [17]. Time-resolved, high-resolution images (Fig. 1), extracted from a digital video sequence recorded at the rate of 15 frames s^{-1}, clearly show the relationship between the reshaping of the particle and the nanotube lift-off. Figure 1 shows a graphene cap attached to the faceted surface of the Ni_3C particle that has started to separate at the top left corner. Further lift-off and growth is accompanied by the appearance and increase in area of another facet that leads to a flattening of the facet under the carbon dome formed after detachment. Immediately before carbon precipitation on the surface and initiation of the next wall formation, the particle shape under the dome became faceted again. Thus, during each carbon wall (tube) nucleation and detachment the particle shape oscillates between having a flat, rounded and faceted top. For each wall of multi-wall CNT formation the process repeats and each new tubular structure is formed via the same lift-off mechanism. Similar shape changes during CNT growth have been reported for Ni and Fe particles earlier, [13, 15, 18] although under different growth conditions.

To quantify the observed dynamics we have measured the time evolution of two suitable geometry parameters: the distance of the growing sp^2-dome from the top catalyst surface, and radius of curvature r of this surface (inset of Fig. 1, right). Results are displayed in the right panel of Fig. 1, for two subsequent domes. The lift-off of the first nanotube, in the interval 1 s to 5 s, is clearly correlated with a divergent r (i.e. vanishing surface curvature ~ 1/r), which clearly indicates the flattening of the cluster top. Around t = 20 s, the catalyst has recovered its original top-surface geometry; the lift-off of a subsequent cap at t = 25 s correlates again with a reduced top-surface curvature.

In order to explain the evolution of the catalyst morphology that we observe, we propose the following mechanism. Carbon originating from the decomposed feedstock populates the catalyst surface at some coverage, $c > 0$ and drastically reduces the surface energy anisotropy, $\gamma_c(\mathbf{n})$, $\mathbf{n}$ being the orientation normal. Consequently, at elevated temperatures the particle adopts nearly spherical shape [19]. This is in contrast to the distinctly polygonal Wulff-construction morphology observed for a metal particle in vacuum, when the energies of pristine surfaces, $\gamma_0(\mathbf{n})$, vary from facet to facet. At sufficiently high values of the coverage, c, the disconnected C-atom population undergoes a type of ordering reaction [20] to bind and form a graphenic sp^2-network. Concurrently, its interaction with metal is reduced to a much weaker van der Waals type while the surface energy anisotropy of the metal (now pristine, underneath the sp^2-dome) becomes high, γ_0. To reduce the overall energy, this surface now tends to flatten, driving redistribution of metal atoms from the domain under the sp^2-cap to the low-γ surface outside. As the flat facet emerges, it separates by some distance from the sp^2-cap, resulting in its lift-off: the sp^2 network thus escapes the short range van der Waals attraction to the metal and permits the unobstructed growth of the nanotube walls. In order to for this mechanism to be plausible, the total energy of the metal-carbon system must in fact be reduced by the morphological changes described. To verify that this is the case, we performed detailed energy computations. This gives a more precise picture of the process, with the energies computed for a series of metal clusters, with their surfaces exposed to carbon adsorption. Further diffusion of C under the primary cap-dome is noted as a surface-energy reducing factor, allowing it to adopt a more rounded shape and

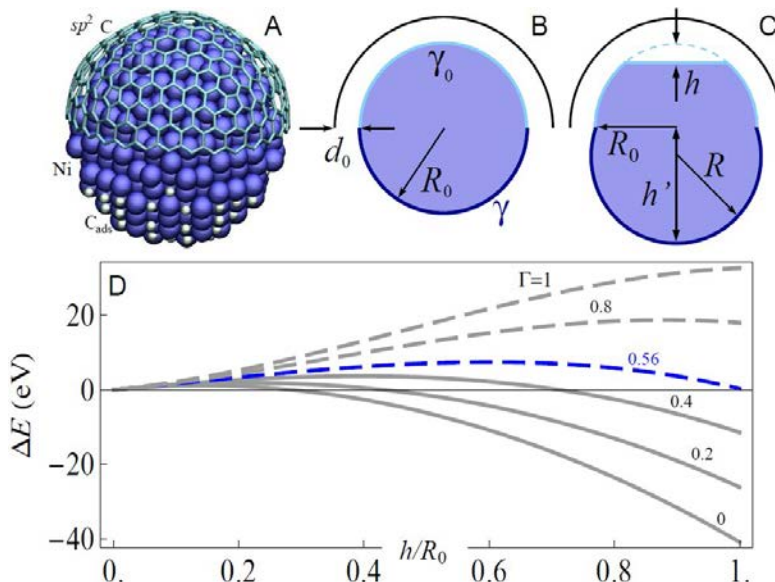eventually leading to the next cycle of a double- or multi-wall nanotube formation.

Fig. 2. Cap-catalyst models: (A) atomistic structure of an example Ni catalyst with sp^2-carbon cap above and chemisorbed C atoms below the equator. (B) A continuum approximation of initial geometry, and then (C) particle faceted under the cap while spherical radius increases to $R > R_0$. (D) Energy change ΔE per Eq. (2), as a function of emerging lift-off gap h in (C), for several normalized surface energy values $\Gamma \equiv \gamma/\gamma_0$.

Phenomenological model. Before calculating the energy for atomistic structures as in Fig. 2A, it is instructive to consider a simpler continuum model. The instant the chemisorbed carbon atoms self-assemble into aromatic sp^2-cap, the cluster underneath becomes free of C, and consequently its surface energy γ_0 is high. The catalyst outside the cap remains at lower surface energy $\gamma \equiv \gamma_c < \gamma_0$ due to unchanged coverage, c. For $\Gamma \equiv \gamma/\gamma_0 < 1$, the total energy can be lowered if the catalyst surface rearranges, flattening by gradually increasing the spacing h under the cap (Fig. 2C), while expanding to a radius $R > R_0$, to some height $h`$ outside the cap, thus preserving the total volume. This requires $v_h(R_0) = v_{h`}(R) - \tfrac{2}{3}\pi R_0^3$, where $v_h(R) \equiv \pi h^2(R-h/3)$, and R_0 remains fixed by the rigid carbon rim. With an identity $h`(2R - h`) = R_0^2$, the value of h fully defines the structure and can serve as an effective reaction coordinate. The energy change includes the surface energy (under the cap and outside) and the van der Waals attraction (approximated as contact interaction, vanishing wherever the catalyst-cap spacing exceeds d_0),

$$\Delta E(h,\Gamma) = \Delta E_{surf}(h,\Gamma) + \Delta E_{vdW}(h). \tag{1}$$

To assess whether the surface energy can drive lift-off, we compute ΔE in the (h,Γ) parameter space, shown in Fig. 2D. With $R_0 = 1.1$ nm, the van der Waals gap $d_0 = 0.2$ nm and an attraction value of 40 meV/atom (obtained by van der Waals density functional theory [21] for graphene on Ni(111) surface), this model predicts a considerable domain where the configuration in Fig. 2C is favored, i.e. $\Delta E < 0$. It also shows that carbon adsorption must reduce the catalyst surface energy ($\Gamma \leq 0.6$) in order to make catalyst reshaping favorable. Should such a condition be satisfied at sufficient coverage and high enough chemical potential μ_C, the top-faceted particle is preferred

4

for some range of h/R_0 and the lift-off mechanism will operate. Quantitative behavior of course changes with a non-contact van der Waals force and other details, better represented in the atomistic analysis below.

Lift-off for a single cap, can be considered for an initially spherical Ni particle of $R_0 \approx 1.1$ nm composed of 531 atoms, which just fits a carbon cap represented by a half of a large fullerene, C_{720}, Fig. 2A. This choice ensures the required number of six pentagons, and corresponds to a starting tube of zigzag chirality (30,0). Interatomic forces are described by the ReaxFF potential [22] as implemented in the LAMMPS simulator [23]; further details of the calculations are given in the Materials and Methods section.

The energetics of the particle-cap system are governed by the underlying potential energy hyper-surface (PES). To maintain a connection with the continuum model, we explore the PES using variables similar to h and γ. Instead of continuous geometry descriptor h, redistribution of particle is now realized in a discrete, layer-by-layer fashion. The initial catalyst-cap orientation is chosen such that removal of material under the cap leads to increased (001) top facet, reshaping the cluster while preserving its crystallinity. We consider seven structures that differ by the number of Ni layers removed from beneath the C cap, with h = 0, Δh, $2\Delta h$, etc. Carbon coverage c is realized by placing N carbon atoms at stable adsorption sites on the exposed surface of cluster. The latter can be considered as a faceted polyhedron with dominant low-index microfacets, viz., {100} {110}, {111}, with smaller areas of high-index "corners" between them. To maintaining approximately constant adsorbate coverage $c \approx$ const, extra adatoms are added for any increase in the exposed catalyst surface.
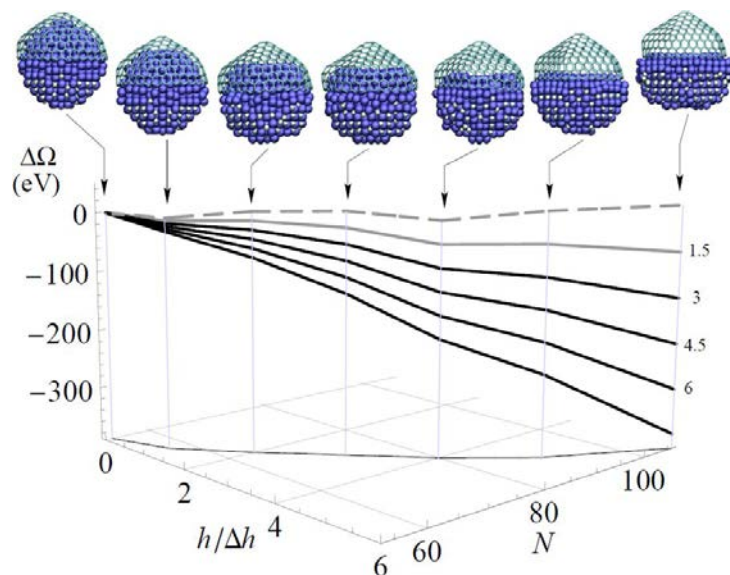

Fig. 3. Grand potential of the catalyst-cap system as a function of lift-off effective coordinate h. Data-point families connected by lines represent the energies for a few values (side labels, in eV) of $\mu_C' \equiv \mu_C - \mu_{C,graphene}$. Topmost and lowest curves indicate the limit cases of $\mu_C = \mu_{C,graphene}$, and $\mu_C = 0$, respectively. The height of the displaced cap h is measured in terms of the interlayer distance along the [001] direction, $\Delta h = a_0/\sqrt{2}$, where a_0 is the lattice constant of bulk fcc Ni.

Since the number of adsorbed carbon atoms N varies in the course of lift-off, the driving force

for the process is due to changes of the grand potential $\Omega = E(N,h) - \mu_C N$, that is,

$$\Delta\Omega = E(N,h) - E(N_0,0) - \mu_C(N-N_0),\qquad\qquad(2)$$

Here $E(N,h)$ is the total energy corresponding to the lift-off magnitude h and the number of adsorbed atoms N; accordingly, $E(N_0,0)$ is the energy before lift-off ($h = 0$ and $N_0 < N$, for equivalent coverage, c). We have calculated $E(N,h)$ for the entire range of (N,h) as independent variables. This is a rich space to analyze the requirements for lift-off, $\Delta\Omega < 0$, as well as its barriers $\Delta\Omega^*$, and the dependencies on adsorption coverage c, which in turn is imposed by the chemical potential at growth conditions (feedstock type, temperature T, partial pressures p_i). A hydrocarbon decomposition quasi-equilibrium, $C_nH_{2m} \leftrightarrow nC + mH_2$, would result in

$$n\mu_C = \mu^0_{C_nH_{2m}} - m\mu^0_{H_2} + k_b T \ln(p_{C_nH_{2m}}/p^m_{H_2}),$$

with k_b the Boltzmann constant, and "0" indicating standard-state chemical potentials [24]. To determine c itself, one needs the adsorption isotherm. For small Ni clusters, $c(\mu_C)$ has been calculated by Amara *et al.* [8] employing tight-binding based grand canonical Monte Carlo simulations; for the present system this would be a daunting task. For our goal, we simply assume some level $c \approx$ const, compute the energies for the representative sequence of varying h, and plot the grand potential change as a function of this effective "reaction-coordinate", Fig. 3. The computed values unambiguously show the reductions in the grand potential at high enough μ_C which quantifies the driving force for the lift-off process.
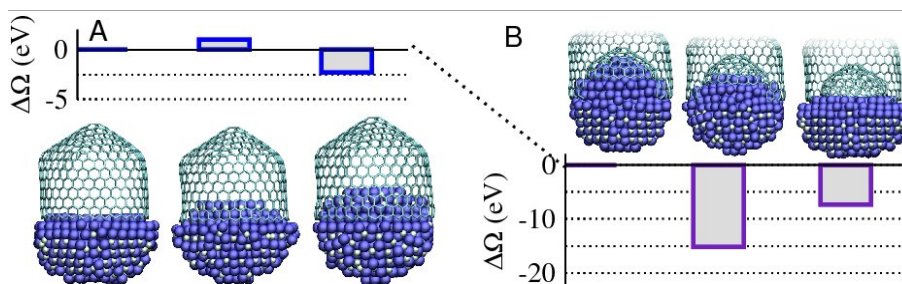

Fig. 4. (A) Reverse cycle in catalyst morphology transformation can be caused by further carbon diffusion underneath the primary C-dome, when chemisorbed C reduces the top-facet surface energy and thus favors overall particle rounding. Shown here are the energies computed for a series of configurations. (B) Onset and lift-off nucleation for a second tube, now a (20,0) zigzag CNT, inside the growing (30,0) tube. For clarity, the outer tube is only partially shown.

Energetics beyond initial lift-off. We now discuss the behaviors of the catalyst-cap system beyond the primary lift-off. Once the cap has lifted and the particle has developed a flat top facet (the last configuration in Fig. 3), further slower diffusion of C through the catalyst-bulk or subsurface can again "contaminate" this top facet and thus decrease its surface energy. This in turn should cause a reverse shape transformation back to a nearly spherical catalyst due to its uniform (and reduced) isotropic surface energy. A series of calculations, Fig. 4, serve to test if such a reversed, second cycle may be energetically favorable. Indeed, the trend for lowering $\Delta\Omega$ in Fig.4 may well be indicative of an interesting stage, possibly playing a key role in multiwall CNT growth. The ultimate prerequisite for such a scenario is the buildup of suitable C population on the catalyst facet that has already "released" a CNT. This would require a driving force, a

gradient in the C adsorbate concentration $|\nabla c|$. Indeed, there have been a number of estimates in the literature, based on the thermochemistry of the Fe-C [25, 26] or Ni-C [24] systems, showing that under typical growth conditions a gradient in the carbon concentration is established. It should be noted, however, that $|\nabla c|$ has to be compliant with sp^2-carbon network nucleation under the dome rather than on the exterior catalyst surface. Possible conditions that may lead to this are: (i) a buffer gas outside attacking the surface and thus preventing nucleation on the exterior surface; (ii) the initial tube serving as a template for subsequent nucleation. These factors clearly warrant further investigation. Once another cap has formed inside the initial, outer nanotube, the same driving force will cause a lift-off. As an indication of the potential for this mechanism to operate, $\Delta\Omega$ is calculated for a few configurations of a (20,0) cap, created from a hemispherically cut C_{320} fullerene, inside the CNT considered in the previous section, and shown in Fig. 4B for $\mu_C = 1.5$ eV.

In conclusion, we have performed *in situ* ESTEM observations and measurements of the geometrical characteristics of the CNT/catalyst system and compared them with empirical-potential atomistic calculations to approximate the dynamics of the morphology and thus gain deeper insight into the CNT nucleation process. The picture that emerges for the CNT nucleation and growth is a rather intriguing one: the metal catalyst can be viewed as an inorganic "heart" of the process, periodically changing its shape in the course of the growth, when a single "heartbeat" is associated with the nucleation and lift-off of a CNT. Oscillating chemical systems are not a novelty [27, 28] in materials science, and CNTs may be just another example of this fascinating phenomenon.

Materials and Methods

Experimental. Samples were prepared by depositing Ni thin films (≈ 1 nm to 2 nm thick, with a small amount of Au) by physical vapor deposition of pristine metal on perforated SiO_2 films supported on 200 mesh Mo TEM grids. These samples were loaded on a TEM heating holder and introduced in to the ESTEM column. Low-magnification scanning transmission electron microscopy (STEM) images show that the films dewetted from the SiO_2 substrate upon heating (>200 °C) to form 4 nm to 7 nm diameter particles. The size of the particles did not change appreciably upon further heating up to the reaction temperatures used (520 °C) but increased slightly after the introduction of C_2H_2. Samples were held at the reaction temperature for ≈ 25 min in order to (i) stabilize the temperature and (ii) complete the reduction of NiO (if present) to Ni in the high vacuum of ESTEM column. C_2H_2 was then introduced in the ESTEM sample area and a pressure ≈ 0.4 Pa was maintained for 15 min.

Theoretical. To represent the variety of interactions in the Ni/C system as large as $\approx 10^3$ atoms, whose energy scales may differ considerably, we have opted for a (semi)empirical potential representation. The recently reported ReaxFF potential is employed for the Ni/C system [22]. We have verified that the reported potential when used in LAMMPS [23] reproduces the basic energetic and structural properties of selected test systems in Ref. [22]. Thus, we have obtained equilibrium lattice constant of fcc Ni a_0=3.61 Å, cohesive energy $\cong 4.5$ eV/atom, and bulk modulus of 153 GPa using the Murnaghan equation of state. For the energies of the three low index surfaces of Ni we find, respectively: $\gamma_{[111]} = 11.8$ V/nm^2, $\gamma_{[110]} = 13.6$ V/nm^2, and $\gamma_{[110]} =$

12.5 V/nm^2. For pristine graphene we find a_0 = 2.48 Å and cohesive energy of 7.85 eV/atom. As a guideline in creating carbon population on low-index Ni surfaces we use the C adsorption energies. Energetics of C adsorption on Ni surfaces and small clusters has been extensively studied from first principles [6, 18, 29-33]. The ReaxFF calculated adsorption energies are in reasonable agreement with first principle results and give C binding in the range 6.7 ev to 7.7 eV. All initial geometries are subject to geometry optimization using the Hessian-free truncated Newton algorithm implemented in LAMMPS [23].

* Corresponding author: aharutyunyan@honda-ri.com

† Corresponding author: biy@rice.edu

DISCLAIMER: *The full description of the procedures used in this manuscript includes identification of certain commercial products and their suppliers. The inclusion of such information should in no way be construed as indicating that such products or suppliers are endorsed by NIST or are recommended by NIST or that they are necessarily the best materials, instruments, software or suppliers for the purposes described.*

1. Dresselhaus, M.S., NT10: Recent Advances in Carbon Nanotube Science and Applications. ACS Nano. **4**: p. 4344-4349.
2. Hersam, M.C., Progress towards monodisperse single-walled carbon nanotubes. Nature Nanotech., 2008. **3**: p. 387-394.
3. Harutyunyan, A.R. and others, Preferential Growth of Single-Walled Carbon Nanotubes with Metallic Conductivity. Science, 2009. **326**: p. 116-120.
4. Ding, F., A.R. Harutyunyan, and B.I. Yakobson, Dislocation theory of chirality-controlled nanotube growth. Proc. Nat. Acad. Sci., 2009. **106**(8): p. 2506-2509.
5. Harutyunyan, A.R., The Catalyst for Growing Single-Walled Carbon Nanotubes by Catalytic Chemical Vapor Deposition Method. J. Nanosci. Nanotechnol., 2009. **9**: p. 2480-2495.
6. Zhang, Q.M. and others, Adsorption of a carbon atom on the Ni$_38$ magic cluster and three low-index nickel surfaces: A comparative first-principles study. Phys. Rev. B, 2004. **69**.
7. Raty, J.Y., F. Gygi, and G. Galli, Growth of Carbon Nanotubes on Metal Nanoparticles: A Microscopic Mechanism from Ab Initio Molecular Dynamics Simulations. Phys. Rev. Lett., 2005. **95**.
8. Amara, H., C. Bichara, and F. Ducastelle, Understanding the Nucleation Mechanisms of Carbon Nanotubes in Catalytic Chemical Vapor Deposition. Phys. Rev. Lett., 2008. **100**.
9. Wang, J.T. and others, Atomistic nucleation and growth mechanism for single-wall carbon nanotubes on catalytic nanoparticle surfaces. Nanotechnology, 2010. **21**(11).
10. Reich, S., L. Li, and J. Robertson, Control the chirality of carbon nanotubes by epitaxial

growth. Chem. Phys. Lett., 2006. **421**: p. 469-472.

11. Amara, H., C. Bichara, and F. Ducastelle, Formation of carbon nanostructures on nickel surfaces: A tight-binding grand canonical Monte Carlo study. Phys. Rev. B, 2006. **73**.

12. Rodriguez-Manzo, J.A. and others, In situ nucleation of carbon nanotubes by the injection of carbon atoms into metal particles. Nature Nanotech., 2007. **2**: p. 307-311.

13. Yoshida, H. and others, Atomic-Scale In-situ Observation of Carbon Nanotube Growth from Solid State Iron Carbide Nanoparticles. Nano Lett., 2008. **8**: p. 2082-2086.

14. Begtrup, G.E. and others, Facets of nanotube synthesis: High-resolution transmission electron microscopy study and density functional theory calculations. Phys. Rev. B, 2009. **79**(20) 205409.

15. Hofmann, S. and others, In situ Observations of Catalyst Dynamics during Surface-Bound Carbon Nanotube Nucleation. Nano Lett., 2007. **7**(3): p. 602-608.

16. Moseler, M. and others, Dynamic Catalyst Restructuring during Carbon Nanotube Growth. ACS Nano, 2010. **4**: p. 7587-7595.

17. Sharma, R., An environmental transmission electron microscope for in situ synthesis and characterization of nanomaterials. J. Materials Res., 2005. **20**.

18. Helveg, S. and others, Atomic-scale imaging of carbon nanofibre growth. Nature, 2004. **427**: p. 426-429.

19. Hong, J.S. and others, Equilibrium shape of nickel crystal. Phil. Mag., 2009. **89**(32): p. 2989-2999.

20. Wiltner, A., C. Linsmeier, and T. Jacob, Carbon reaction and diffusion on Ni(111), Ni(100), and Fe(110): Kinetic parameters from x-ray photoelectron spectroscopy and density functional theory analysis. J. Chem. Phys., 2008. **129**, 084704.

21. Vanin, M. and others, Graphene on metals: A van der Waals density functional study. Phys. Rev. B, 2010. **81**(8) 0811408(R).

22. Mueller, J.E., A.C.T. van Duin, and W.A. Goddard, Development and Validation of ReaxFF Reactive Force Field for Hydrocarbon Chemistry Catalyzed by Nickel. J. Phys. Chem. C, 2010. **114**: p. 4939-4949.

23. Plimpton, S.J., Fast Parallel Algorithms for Short-Range Molecular Dynamics. J. Comp. Phys., 1995. **117**: p. 1-19.

24. Snoeck, J.W., G.F. Froment, and M. Fowles, Filamentous Carbon Formation and Gasification: Thermodynamics, Driving Force, Nucleation and Steady-State Growth. J. Catal., 1997. **169**: p. 240-249.

25. Parmon, V.N., Fluidization of the active component of catalysts in catalytic formation of carbon assisted by iron and nickel carbides. Catal. Lett., 1996. **42**: p. 195-199.

26. Klinke, C., J.M. Bonard, and K. Kern, Thermodynamic calculations on the catalytic growth of multiwall carbon nanotubes. Phys. Rev. B, 2005. **71**.

27. Kuznetsov, V.L., A.N. Usol'tseva, and Y.V. Butenko, Mechanism of Coking on Metal Catalyst Surfaces: I. Thermodynamic Analysis of Nucleation. Kinet. Catal., 2003. **44**: p. 726-734.

28. Oh, S.H. and others, Oscillatory Mass Transport in Vapor-Liquid-Solid Growth of Sapphire Nanowires. Science, 2010. **330**(6003): p. 489-493.

29. Hong, S., Y.H. Shin, and J. Ihm, Crystal shape of a Nickel particle related to carbon nanotube growth. Jpn. J. Appl. Phys., 2002. **41**(10): p. 6142-6144.

30. Abild-Pedersen, F., et al., Mechanisms for catalytic carbon nanofiber growth studied by ab initio density functional theory calculations. Phys. Rev. B, 2006. **73**.

31. Shin, Y.H. and S. Hong, Carbon diffusion around the edge region of nickel nanoparticles.

Appl. Phys. Lett., 2008. **92**(4).

32. Yazyev, O.V. and A. Pasquarello, Effect of Metal Elements in Catalytic Growth of Carbon Nanotubes. Phys. Rev. Lett., 2008. **100**.

33. Kalibaeva, G., et al., Ab Initio Simulation of Carbon Clustering on an Ni(111) Surface: A Model of the Poisoning of Nickel-Based Catalysts. J. Phys. Chem. B, 2006. **110**: p. 3638-3646.